# Accepted Manuscript

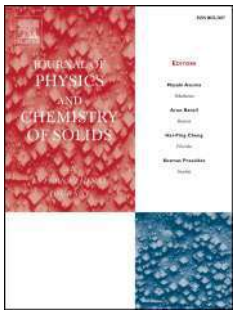

Effects of $Zn^{2+}$-$Zr^{4+}$ ions on the structural, mechanical, electrical, and optical properties of cobalt ferrites synthesized via the sol–gel route

S.S. Desai, S.M. Patange, A.D. Patil, S.K. Gore, S.S. Jadhav

PII: S0022-3697(18)33333-X

DOI: https://doi.org/10.1016/j.jpcs.2019.05.024

Reference: PCS 9027

To appear in: *Journal of Physics and Chemistry of Solids*

Received Date: 7 December 2018

Revised Date: 14 May 2019

Accepted Date: 15 May 2019

Please cite this article as: S.S. Desai, S.M. Patange, A.D. Patil, S.K. Gore, S.S. Jadhav, Effects of $Zn^{2+}$-$Zr^{4+}$ ions on the structural, mechanical, electrical, and optical properties of cobalt ferrites synthesized via the sol–gel route, *Journal of Physics and Chemistry of Solids* (2019), doi: https://doi.org/10.1016/j.jpcs.2019.05.024.

This is a PDF file of an unedited manuscript that has been accepted for publication. As a service to our customers we are providing this early version of the manuscript. The manuscript will undergo copyediting, typesetting, and review of the resulting proof before it is published in its final form. Please note that during the production process errors may be discovered which could affect the content, and all legal disclaimers that apply to the journal pertain.


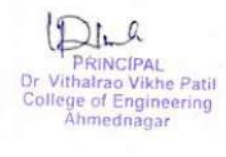

ACCEPTED MANUSCRIPT

# Effects of $Zn^{2+}$- $Zr^{4+}$ ions on the structural, mechanical, electrical, and optical properties of cobalt ferrites synthesized via the sol–gel route

S. S. Desai[1], S. M. Patange[2], A. D. Patil[3], S. K. Gore[4], S. S. Jadhav[4*]

[1]*Dept. of Physics, Dr. Vithalrao Vikhe Patil College of Engineering, Ahmednagar, M. S., India*
[2]*Materials Research Laboratory, Shrikrishna Mahavidyalaya, Gunjoti 413613, M. S., India*
[3]*Deshbhakt Anandrao Balawantrao Naik Arts and Science College, Chikhali, M. S., India*
[4]*D. S. M.'s Arts, Commerce and Science College, Jintur, 431509, M. S., India*

**Corresponding author: santosh.jadhav28@yahoo.com*

**Abstract**

In the present study, we examined the effects of doping with Zn-Zr on the structural, optical, electrical, and mechanical properties of cobalt ferrite. Nanocrystalline cobalt ferrites comprising $CoZn_xZr_xFe_{2-2x}O_4$ (x = 0.0 to 0.4, $\Delta x = 0.1$) were prepared via the sol–gel route. X-ray diffraction analysis indicated the formation of a spinel phase in the ferrites. An additional $ZrO_2$ phase was observed for x = 0.3. Characteristic absorption bands at frequencies of 580–610 $cm^{-1}$ and 375–400 $cm^{-1}$ related to spinel structures were observed in the Fourier transform infrared FTIR spectra obtained for the ferrites. The elastic constants decreased as the Zn-Zr contents increased. The longitudinal and shear velocities of ultrasound through the ferrite materials were measured using the ultrasonic pulse transmission method. The variations in the ultrasound velocities could be attributed to the changes in density. The dielectric parameters ε′ (dielectric constant) and tanδ (dielectric loss tangent) were analyzed as functions of the frequency and Zn-Zr composition. Both ε′ and tanδ decreased as the frequency and Zn-Zr contents increase. The variations in the values of parameters ε′ and tanδ were explained using Maxwell–Wagner interfacial polarization according to Koops phenomenological theory. The values of the activation energy and Curie temperature were calculated based on plots of the thermal variation in the direct current resistivity. The activation energy values indicated that electron hopping was the mechanism responsible for conduction in the ferrites.

PRINCIPAL
Dr. Vithalrao Vikhe Patil
College of Engineering
Ahmednagar

**Keywords**: Curie temperature; Dielectric property; Direct current resistivity; Elastic Property; Ferrite; Fourier transform infrared; Sol–gel route.

## 1. Introduction

Recently, spinel ferrites have been developed as versatile ceramic magnetic materials with special optical, magnetic, electrical, photocatalytic, and biomedical properties [1-5]. The complex structures of spinels are due to their high compositional variability where solid solutions can be prepared with various metal cations. Spinel ferrites have close-packed cubic crystal structures where anions ($O^{2-}$) are amalgamated with cations ($Fe^{3+}$and divalent metal ions) in two sub-lattices, such as tetrahedral (A) and octahedral [B] sites [6-8]. Many attempts have been made to modify the electrical and elastic properties of ferrites by substituting divalent, trivalent, and tetravalent cations for divalent metal ions or trivalent $Fe^{3+}$ ions [9-11]. The cobalt ferrite $CoFe_2O_4$ is a unique ferrite with high magnetocrystalline anisotropy of 14 KJ/$m^3$ [12] and an inverse spinel structure with cations distributed along the (A) and [B] site as $(Co_{1-x}Fe_x)^A$ $[Co_xFe_{2-x}]^B$, where x is an inversion parameter. The substitution of $Zn^{2+}$ into $CoFe_2O_4$ allows ferrites to be obtained with suitable magnetic and electrical properties for various applications such as magnetic storage media and microwave electronics [13, 14].

Substitution with $Zr^{4+}$ modifies the magnetic and structural properties of cobalt ferrite [15, 16]. Thus, significant changes in terms of the saturation magnetization, coercivity, and magnetic anisotropy of cobalt ferrite were obtained after substitution with $Zr^{4+}$ by Reddy et al. [17]. $Zr^{4+}$ substituted cobalt ferrite is a suitable material for magnetostrictive applications [18]. Cobalt ferrites doped with Zn-Zr have many technological applications at high frequencies due to their low magnetic losses [19-20]. In spinel ferrites, $Zn^{2+}$ ions occupy the tetrahedral (A) sites [21] whereas $Zr^{4+}$ ions occupy both the (A) and [B] sites [22]. Combinations of divalent and tetravalent ions such as Zn-Ti [23], Zn-Sn [24], and Zn-Mo [25] have been used to dope ferrite systems in many studies. In particular, it was shown that simultaneous doping with Zr-Mg to replace $Fe^{3+}$ ions modified the electrical and structural properties of cobalt ferrites [26].

Various approaches have been used to prepare nanoferrites, such as co-precipitation [27], mechanochemical reaction [28], citrate gel [29], precursor [30], sol–gel [31], hydrothermal [32], chemical spray [33], and

microwave combustion methods [34, 35]. In particular, the sol–gel autocombustion method is the most suitable, effective, and inexpensive [36] method for preparing ferrite nanoparticles. The other advantages of this method include the production of homogeneous and uniformly distributed particles with relatively smaller sizes compared with other approaches, such as the co-precipitation and citrate gel methods [37]. The production of spinel ferrites with a single phase is an important feature of the sol–gel auto combustion method, particularly when preparing spinel ferrites with various cations at the (A) and [B] sites [38].

Analyzing the mechanical behavior of ferrites is very important for understanding the nature of the inter-atomic and ionic forces in ferrites. Determining the mechanical properties of ferrites can facilitate the selection of suitable ferrites for industrial applications [39]. In particular, the elastic behavior of a material is important for determining the nature of the binding forces and thermal properties, such as the specific heat and Debye temperature. The mechanical properties of ferrites are also crucial, such as the strength of a material under various strained conditions [40].

In the present study, we determined how the physical properties of cobalt ferrites change after simultaneous substitution with $Zn^{2+}$-$Zr^{4+}$ for two $Fe^{3+}$ cations because both $Zn^{2+}$ and $Zr^{4+}$ have strong preferences for the tetrahedral (A) site, but they can replace $Fe^{3+}$ ions at both the (A) and [B] sites. The incorporation of $Zn^{2+}$ and $Zr^{4+}$ cations into $CoFe_2O_4$ ferrite could yield ferrites with enhanced elastic and electrical properties. Thus, we synthesized cobalt ferrites nanoparticles doped with Zn-Zr via the sol–gel auto-combustion method and investigated the effects of Zn-Zr doping on the structural, optical, mechanical, and electrical properties of the cobalt ferrites.

## 2. Experimental Methods

### 2.1. Synthesis

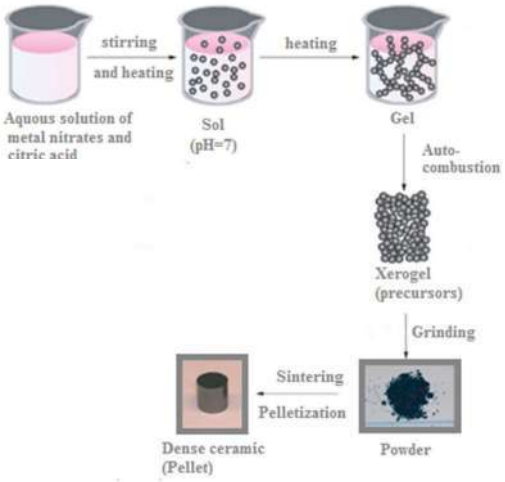

**Fig. 1.** Flow chart illustrating the sol–gel synthesis of $CZ^2FO$.

Figure 1 illustrates the sol–gel autocombustion method employed for synthesizing Zn-Zr substituted cobalt ferrites with the chemical formula $CoZn_xZr_xFe_{2-2x}O_4$ ($CZ^2FO$), where x = 0.0 to 0.4. The chemicals used for synthesizing the ferrites comprised nitrates of the compositional metal elements, ammonia solution, and citric acid, where all of the reagents were analytical grade. The solutions were prepared in deionized water by dissolving the metal nitrate salts in stoichiometric amounts for all of the elements. A molar ratio of 1:2 was maintained for the divalent and trivalent ions. An aqueous solution of citric acid was prepared. The aqueous solutions of metal nitrates and citric acid were mixed together, and the mixed solution was stirred continuously for 30 min with a magnetic stirrer. The pH of the solution was maintained at 7 by adding ammonium hydroxide solution [41]. The solution was stirred and heated simultaneously at 100°C to obtain a thick solution comprising the sol phase. Continuous heating of the sol converted it into a viscous gel, which automatically ignited to yield the precursor known as the xerogel. The precursor was converted into a powder by grinding in an agate mortar. The powder was annealed at 650°C for 5 h in a furnace at a constant temperature under an air atmosphere to obtain the dense ceramic ferrite material.

### 2.2. Measurements

The structural characteristics of the ferrites were determined by X-ray diffraction (XRD) and Fourier transform infrared (FTIR) spectroscopy. The XRD patterns were recorded in the 2θ range from 20° to 80° using an XRD instrument (Philips X'Pert model) with Cu-Kα radiation at λ = 1.54056 Å and with a scanning rate of 10° per second at room temperature. The FTIR spectra were recorded in the wave number range from 300–1100 $cm^{-1}$ using an infrared spectrometer (Perkin Elmer model 783). The mechanical properties were measured using the ultrasonic pulse transmission method. The longitudinal and shear wave velocities ($V_l$ and $V_s$) were obtained for all of the samples at room temperature. The ultrasonic waves were generated using lead zirconate titanate (PZT) crystals at 124.6 KHz. The measurements were obtained with an accuracy of ±5 m/s using the interferometer. An impedance analyzer (HIOKI 3532-50) was used to obtain electrical measurements in the frequency range from 50 Hz to 5 MHz at room temperature.

The two-probe method was used to measure the direct current (DC) resistivity in the temperature range from 300 K to 700 K. Disk-shaped pellets were prepared with a diameter of 10 mm and thickness of 3 mm. The samples were held between the two electrodes in a sample holder. A specially designed sample holder was used to measure the resistivity. The pellets were rubbed with zero grade emery paper to obtain parallel smooth faces. A thin layer of silver paste was applied to both of the flat surfaces of the pellets to obtain secure electrical contacts. The sample holder containing the sample was placed in an electric furnace. The temperature in the furnace was modulated as required. A suitable thermocouple (chromel-alumel) was used to measure the temperature of the sample. The resistance of each sample was measured over a regular temperature interval with steps of 10 K.

## 3. Results

### 3.1. XRD Analysis

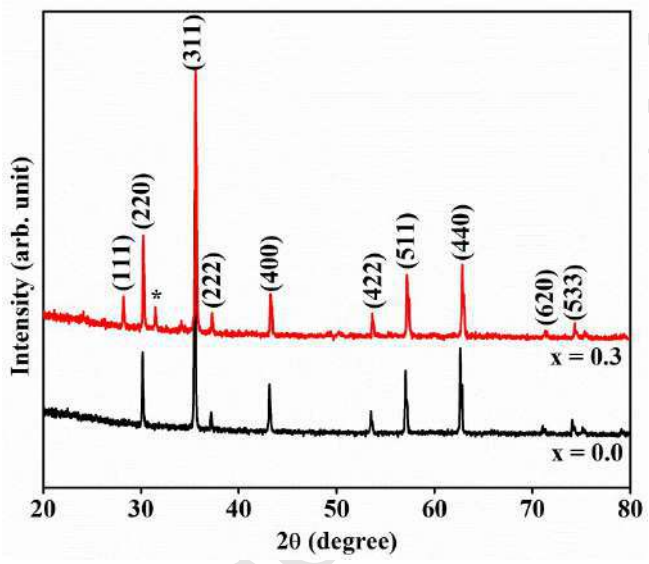


**Fig. 2.** X-ray diffraction patterns obtained for typical $CZ^2FO$ samples where x = 0 and x = 0.3. The symbol * indicates (111) for $ZrO_2$.

The typical XRD patterns obtained for $CZ^2FO$ where x = 0 and 0.3 are shown in Fig. 2. The peaks observed in the XRD patterns were indexed using Bragg's law. The sequences and Miller indices of the peaks matched with JCPDS file No. 22-1086 for cobalt ferrite, thereby indicating the formation of cubic crystals comprising spinel phase ferrites with space group Fd3m. The extra peak observed at 31.44° for the ferrite where x = 0.3

corresponded to the peak (111) for $ZrO_2$ (zirconium oxide) according to JCPDS file No. 37-1484 [42, 43]. XRD analysis was performed to calculate the lattice parameters (a) for the ferrites. Table 1 shows that the lattice parameter increased with the amount of Zn-Zr substituted (x). The replacement of two $Fe^{3+}$ (0.67Å) ions by two $Zn^{2+}$ (0.82 Å) and $Zr^{4+}$ (0.80 Å) ions with larger radii increased the size of the unit cell, thereby increasing the value of a [44, 45].

The bulk density values of the ferrites were calculated using the relationship [47]:

$$d_m = m/\pi r^2 h, \quad (1)$$

where m, r, and h are the mass, radius, and thickness of the ferrite pellet, respectively. The values obtained are shown in Table 1. The increases in the bulk density values indicated that the densities of the ferrite samples increased after the substitution of Zn-Zr into the $CZ^2FO$ ferrites.

The bond lengths (tetrahedral and octahedral), tetrahedral edges, and octahedral edges (shared and unshared) were calculated using the following formulae [47].

$$d_{AX} = (u - 1/4)a\sqrt{3} \quad (2)$$

$$d_{BX} = a(3u^2 - 11u/4 + 43/64)^{1/2} \quad (3)$$

$$d_{AXE} = (2u - 1/2)a\sqrt{2} \quad (4)$$

$$d_{BXE(\textbf{shared})} = (1-2u)a\sqrt{2} \quad (5)$$

$$d_{BXE(\textbf{unshared})} = a(4u^2 - 3u + 11/16)^{1/2} \quad (6)$$

The values obtained are listed in Table 1. The increases in the bond lengths and edges as the Zn-Zr content increased were due to the increases in the lattice parameters. The increases in the bond length values were due to the increases in the amount of $Zn^{2+}$ (0.82Å) and $Zr^{4+}$ (0.80Å) ions with larger ionic radii that replaced the relatively smaller $Fe^{3+}$ ions (0.67Å). Site occupancy by the incorporated $Zn^{2+}$ and $Zr^{4+}$ ions was responsible for the increases in the tetrahedral and octahedral edges. In the $CZ^2FO$ ferrites, $Zn^{2+}$ occupied the tetrahedral site whereas

$Zr^{4+}$ occupied the octahedral site after replacing the $Fe^{3+}$ ions. Due to the ion replacements at these sites, the tetrahedral and octahedral edges increased with the amount of substituted Zn-Zr [47].

**Table 1.** Lattice constant (a), tetrahedral bond ($d_{AX}$), octahedral bond ($d_{BX}$), tetrahedral edge ($d_{AXE}$), and octahedral edge ($d_{BXE}$) (shared and unshared) values determined for $CZ^2FO$.

| x | a (Å) | ρ (g/cc) | Bond Lengths (Å) | | Edges (Å) | | |
|---|---|---|---|---|---|---|---|
| | | | | | $d_{AXE}$ | $d_{BXE}$ | |
| | | | $d_{AX}$ | $d_{BX}$ | | Shared | Unshared |
| 0.0 | 8.375 | 4.076 | 1.900 | 2.047 | 3.103 | 2.818 | 2.969 |
| 0.1 | 8.383 | 4.161 | 1.902 | 2.049 | 3.106 | 2.821 | 2.971 |
| 0.2 | 8.395 | 4.204 | 1.904 | 2.051 | 3.109 | 2.825 | 2.975 |
| 0.3 | 8.402 | 4.331 | 1.906 | 2.053 | 3.113 | 2.828 | 2.978 |
| 0.4 | 8.412 | 4.501 | 1.908 | 2.055 | 3.116 | 2.830 | 2.981 |

### 3.2. FTIR Analysis

ACCEPTED MANUSCRIPT

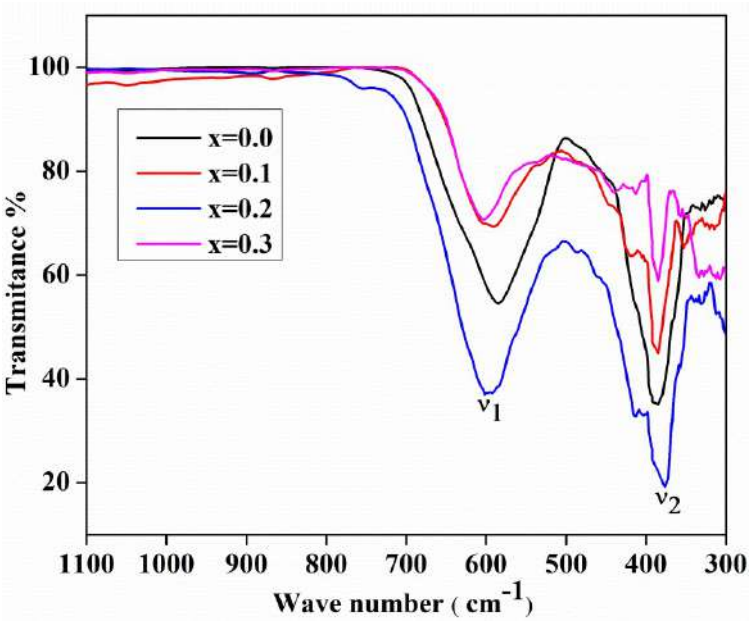


**Fig. 3.** Fourier transform infrared spectra obtained for $CZ^2FO$ with different Zn-Zr contents (x).

The infrared absorption spectra were measured for the synthesized samples using the KBr pellet method over the range from 300–1100 $cm^{-1}$ at room temperature. The FTIR spectra obtained for all of the samples are shown in Fig. 3. Transmission bands $\nu_1$ and $\nu_2$ were observed at around 600 and 400 $cm^{-1}$, respectively. The measured bands indicated the characteristic ferrospinel bands representing stretching vibrations due to the interactions between the oxygen atom and cations at the tetrahedral and octahedral sites. Significant changes occurred in the $\nu_1$ band where it shifted from lower to higher frequencies as the amount of doping with Zn-Zr ions increased, which was due to the stretching of Fe-O bonds. This shift in the band position may have been due to the replacement of Fe with Zn-Zr [38]. The location of absorption band $\nu_2$ at a lower frequency may have been related to oxygen–metal (octahedral) vibrations. The band positions and their values are shown in Table 2. According to Table 2, the $\nu_1$ and $\nu_2$ bands gradually shifted toward the higher frequency side because the $Zn^{2+}$ ions occupied the tetrahedral A-site in the ferrite lattice.

The relative ratio of the line positions for $\nu_1$ and $\nu_2$ is given by the relationship [48]:

$$\frac{\nu_1}{\nu_2} = \frac{\sqrt{2}K_t}{K_0}, \qquad (7)$$

where $K_t$ and $K_o$ are force constants due to the displacement of cations–oxygen at the (A) and (B) sites. The ratio of the force constants was calculated using equation (6) and the values obtained are given in Table 2. The ratios of the force constants were ≈1, thereby indicating that expansion of the octahedral (B) sites and compression of the tetrahedral (A) sites were not the same. The splitting of the bands indicated the replacement of cations at the (A) and [B] sites.

**Table 2**. Bands positions ($\nu_1$ and $\nu_2$), ratio of force constant ($K_t/K_o$), and Poisson's ratio ($\sigma$) for $CZ^2FO$ samples.

| Composition (x) | Bands Position ($cm^{-1}$) | | $K_t/K_o$ | Poisson Ratio |
|---|---|---|---|---|
| | $\nu_1$ | $\nu_2$ | | |
| 0.0 | 584 | 376 | 1.09 | 0.249 |
| 0.1 | 592 | 384 | 1.09 | 0.258 |
| 0.2 | 597 | 388 | 1.08 | 0.260 |
| 0.3 | 607 | 393 | 1.09 | 0.268 |

### 3.2. Mechanical Properties

The longitudinal ($v_l$) and shear ($v_s$) ultrasonic wave velocities were measured with the ultrasonic pulse transmission technique at room temperature.

ACCEPTED MANUSCRIPT

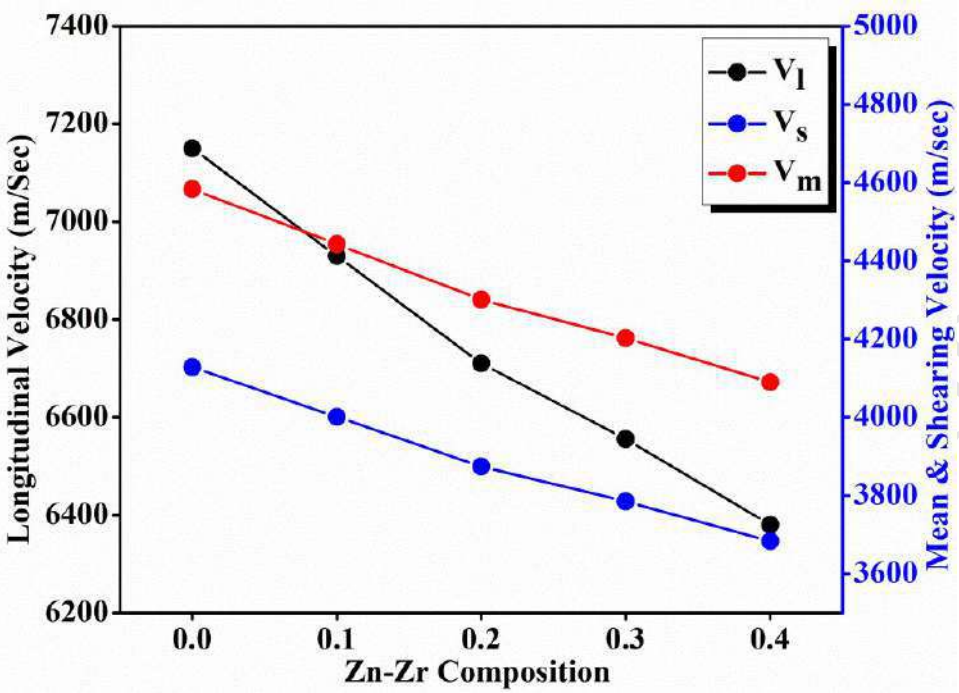


**Fig. 4.** Longitudinal velocity ($v_l$), shearing velocity ($v_s$), and mean velocity ($v_m$) of $CZ^2FO$ with different Zn-Zr contents (x).

Figure 4 shows the variations in the longitudinal wave velocity and mean velocity according to the Zn-Zr contents, where the wave velocity clearly decreased as the Zn-Zr contents (x) increased. The decrease in the wave velocity was due to the increase in the bulk density of the material. The shearing wave velocity was always less than the longitudinal velocity. The mean sound velocity was calculated using the relationship reported by Algude et al. [49] and the mean velocity clearly decreased as the Zn-Zr contents (x) increased.

The longitudinal modulus (L), Young's modulus (E), rigidity modulus (G), Poisson's ratio (σ), and bulk modulus (K), were calculated using the experimental values of $v_l$, $v_s$, and bulk density (ρ) according to the following relationships [49].

$$L = \rho v_l^2 \quad (8)$$

$$E = 3GK/(3K+G) \quad (9)$$

$$G = \rho v_s^2 \quad (10)$$

$$K = \frac{\rho}{3}(3v_l^2 - 4v_s^2) \quad (11)$$

$$\sigma = (E/2G)-1 \qquad (12)$$

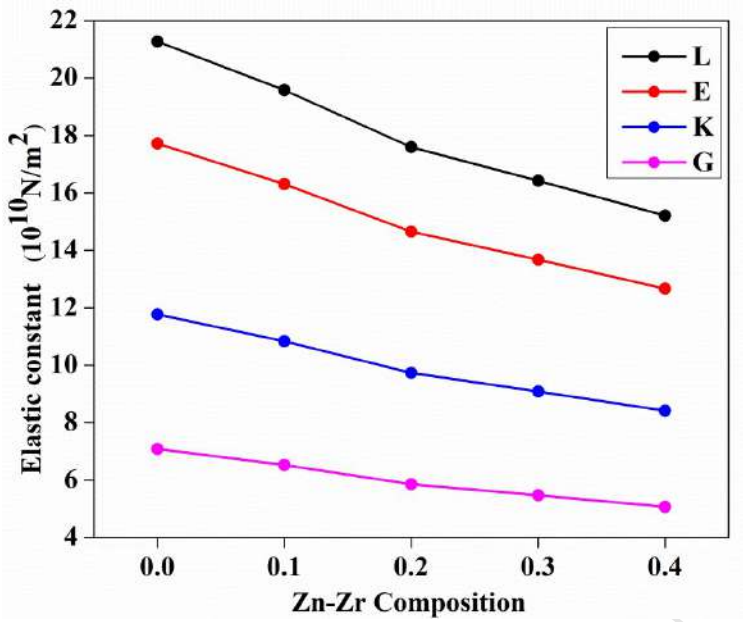


**Fig. 5.** Variations in Young's modulus (E), longitudinal modulus (L), bulk modulus (K), and modulus of rigidity (G) for $CZ^2FO$ with different Zn-Zr contents (x).

The variations in all of the moduli with the Zn-Zr contents (x) are shown in Fig. 5. Clearly, all of the moduli decreased as the Zn-Zr contents (x) increased. The decreases in the values were as follows: L from $21.3 \times 10^{10}$ to $15.2 \times 10^{10}$ N/m$^2$, E from $17.8 \times 10^{10}$ to $12.7 \times 10^{10}$ N/m$^2$, K from $11.8 \times 10^{10}$ to $8.4 \times 10^{10}$ N/m$^2$, and G from $7.1 \times 10^{10}$ to $5.1 \times 10^{10}$ N/m$^2$. The decreases were due to the replacement of the Fe ions with high values for all of the moduli by Zn-Zr ions with comparatively low values for all of the moduli. The elastic properties of materials depend on the crystal structure, bonding stiffness, hardness, and strength. The elastic moduli decreased slightly as the lattice expanded due to the replacement of the Fe ions by Zn-Zr ions. Table 2 shows that the Poisson's ratio values were almost constant ($\sigma \approx 0.26$) for all of the samples tested, in a similar manner to other ferrites [25]. The value of σ varied in the range from –1 to 0.5, thereby providing theoretical evidence of isotropic elasticity.

The Debye temperatures of all the samples were obtained from the mean velocities as [49]:

$$\theta_E = \frac{h}{k}\left(\frac{3q\rho N}{4\pi M}\right)^{\frac{1}{3}} \times v_m, \qquad (13)$$

where h, q, ρ, N, k, and M are Planck's constant, the number of atoms in the ferrite molecule, material density of

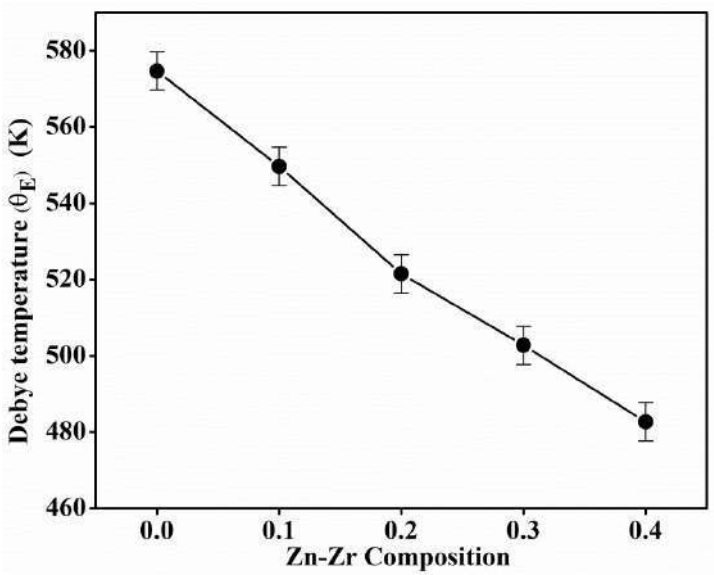


**Fig. 6.** Variations in the Debye temperature ($\theta_E$) for $CZ^2FO$ with different Zn-Zr contents (x).

the ferrite, Avogadro's number, Boltzmann's constant, and molecular weight of the ferrite, respectively. Figure 6 shows the variations in the Debye temperature as the Zn-Zr contents (x) increased. Clearly, the Debye temperature decreased as the Zn-Zr contents (x) increased due to the decrease in the mean velocity. The characteristic temperature of a solid at which most of the vibration modes of the solid are agitated is recognized as the Debye temperature. The decrease in the Debye temperature for the $CZ^2FO$ ferrites indicated a decrease in the rigidity as the Zn-Zr contents (x) increased. The vibrations were increased due to the substitution of Zn-Zr in the Co ferrite.

### 3.3. Electrical Properties

#### 3.3.1. Dielectric Properties

The dielectric properties comprising the dielectric loss tangent (tanδ) and dielectric constant (ε′) were calculated based on the capacity values measured for the materials in the frequency range from 50 Hz to 5 MHz. The variations in ε′ with the frequency of the electric field are shown in Fig. 7. According to Fig. 7, ε′ decreased as the frequency increased but remained almost constant at higher frequencies. Similar results were reported for Co-Ni ferrites doped with Zr-Co [50]. The decrease in the dielectric constant at higher frequencies conformed with the Maxwell–Wagner mechanism. The ferrite materials comprised conducting grains with non-conducting grain boundaries. There were more grains in the conducting layer than the non-conducting layer. Polarization and

conduction existed in the ferrites due to the hopping of electrons from $Fe^{3+}$ to $Fe^{2+}$ ions. The dielectric polarization decreased as the electric field frequency increased and then reached a constant value at a certain frequency beyond which the hopping of electrons could not follow the applied field [51].

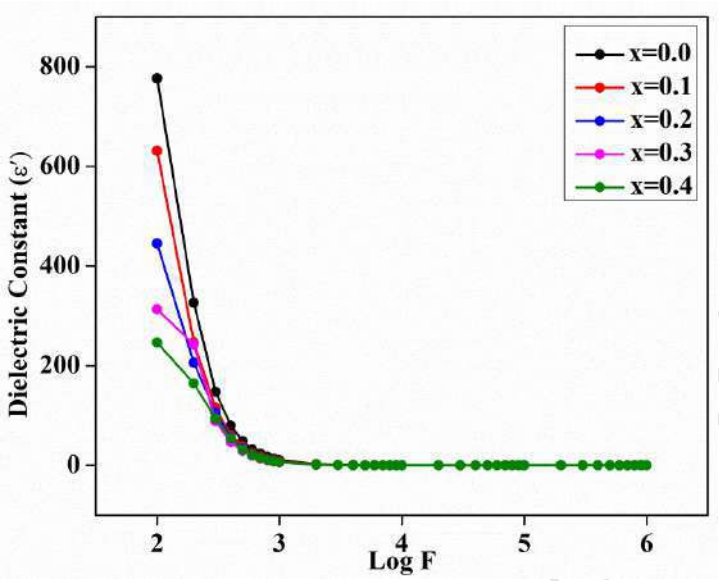


**Fig. 7.** Variations in the dielectric constant (ε′) with the frequency (logF) for $CZ^2FO$ with different Zn-Zr contents (x).

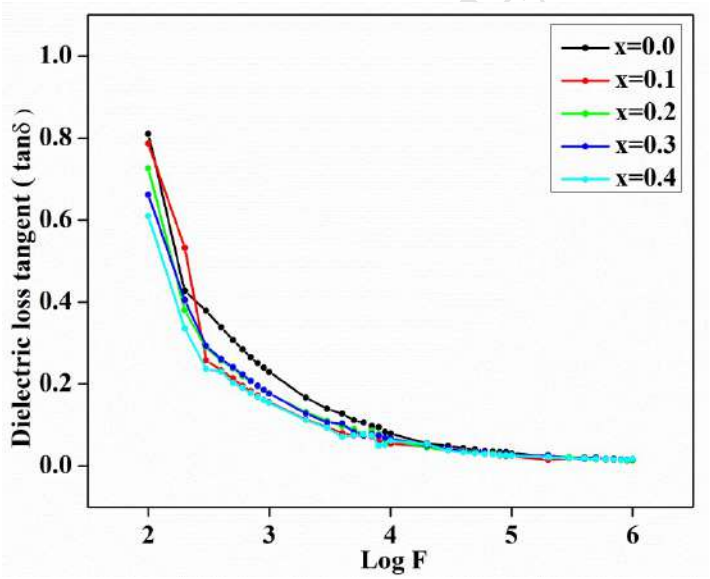


**Fig. 8.** Variations in the dielectric loss tangent with log F for $CZ^2FO$ with different Zn-Zr contents (x).

Figure 8 shows the variations in the dielectric loss tangent (tanδ) with the frequency of the electric field. The values of tanδ decreased as the applied electric field frequency increased. The Maxwell–Wagner model could be used to explain the variations in the dielectric loss tangent. The substitution of Zn-Zr for $Fe^{3+}$ decreased the hopping mechanism from $Fe^{3+}$ to $Fe^{2+}$ ions. The dielectric loss tangent appeared due to the lag in the polarization behind the applied electric field. The value of tanδ depended on the structural inhomogeneities and the impurities present in the ferrite samples. The maximum value obtained for tanδ was 0.8. The small values for the dielectric loss tangent indicated the structural perfection of the ferrite samples synthesized via the sol–gel route [52].

**Table 3.** Dielectric constant (ε') and dielectric loss tangent (tanδ) determined for $CZ^2FO$ at different frequencies.

| Frequency | Dielectric constant (ε') | | | | | Dielectric loss tangent (tanδ) | | | | |
|---|---|---|---|---|---|---|---|---|---|---|
| | x = 0 | x = 0.1 | x = 0.2 | x = 0.3 | x = 0.4 | x = 0 | x = 0.1 | x = 0.2 | x = 0.3 | x = 0.4 |
| 1 KHz | 776.63 | 630.992 | 445.139 | 313.193 | 246.573 | 0.810 | 0.787 | 0.726 | 0.662 | 0.609 |
| 10 KHz | 10.238 | 7.632 | 6.725 | 5.792 | 6.425 | 0.229 | 0.185 | 0.177 | 0.177 | 0.154 |
| 100 KHz | 0.0425 | $3.01 \times 10^{-2}$ | $2.65 \times 10^{-2}$ | $2.52 \times 10^{-2}$ | $2.88 \times 10^{-2}$ | 0.079 | 0.067 | 0.065 | 0.061 | 0.061 |
| 1 MHz | $1.80 \times 10^{-4}$ | $1.43 \times 10^{-4}$ | $1.28 \times 10^{-4}$ | $1.05 \times 10^{-4}$ | $1.25 \times 10^{-4}$ | 0.032 | 0.027 | 0.025 | 0.025 | 0.026 |
| 10 MHz | $8.24 \times 10^{-7}$ | $8.63 \times 10^{-7}$ | $7.92 \times 10^{-7}$ | $6.98 \times 10^{-7}$ | $5.54 \times 10^{-7}$ | 0.014 | 0.017 | 0.016 | 0.014 | 0.015 |

The values of the dielectric constant (ε') and loss tangent (tanδ) at frequencies of 1, 10, and 100 KHz, and 1 and 10 MHz for all of the $CZ^2FO$ ferrites are shown in Table 3. The differences in the values of ε' and tanδ as the Zn-Zr contents (x) increased were greater up to frequencies of 100 KHz. At high frequencies ≥1 MHz, the differences in the values were negligibly small. The values of both ε' and tanδ decreased with the frequency as the Zn-Zr contents (x) increased. The decrease in ε' as the Zn-Zr contents (x) increased was due to the increase in the resistivity, as shown in Fig. 9 [51].

### 3.3.1. DC Resistivity

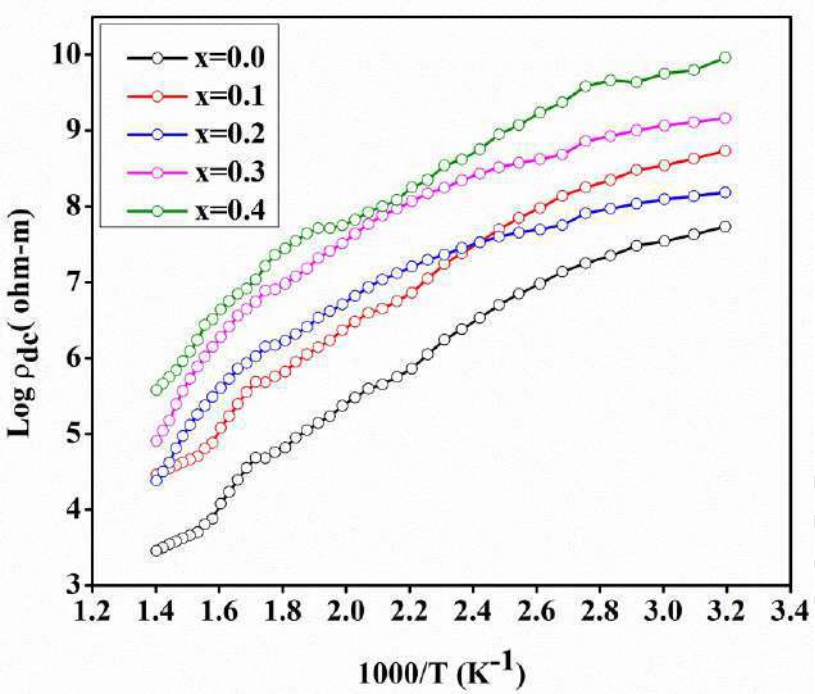


**Fig. 9.** Variations in direct current resistivity with temperature for $CZ^2FO$ with different Zn-Zr contents (x).

The dependences of the electrical resistivity on the composition and temperature for the samples were studied using the two-probe technique. The resistivity values were calculated using the following equation:

$$\rho = R.A / l, \qquad (14)$$

where A is the cross-sectional area of the pellet, R is the measured resistance, and l is thickness of the pellet.

Figure 9 shows the variations in the DC resistivity with temperature for the cobalt ferrites doped with Zn-Zr. The high conductivity values determined for the ferrites were due to the presence of both $Fe^{3+}$ and $Fe^{2+}$ ions in the crystallographically equivalent sites. The low resistivity of ferrites was related to the occupancy of divalent metal ions and trivalent iron ions at the octahedral B-sites. The doped $Zn^{2+}$ and $Zr^{4+}$ ions occupied the (A) and [B] sites, respectively, whereas the $Fe^{3+}$ and $Fe^{2+}$ ions occupied the (A) and [B] sites. The conduction in the ferrites occurred via the hopping of electrons between $Fe^{2+}$ and $Fe^{3+}$ ions. The increasing concentration of Zn-Zr in $CZ^2FO$ increased the amount of $Fe^{2+}$ ions to increase the hopping between Fe ions, and thus the DC resistivity decreased [17]. The activation energy was calculated using the Arrhenius equation ($\rho = \rho_0 \exp [\Delta E / kT]$) and the Curie temperature was calculated from the plots of log$\rho$ versus 1000/T. The activation energy and Curie

temperature are shown in Table 4. The activation energy was $\Delta E < 0.2$ eV for all of the ferrite samples, thereby indicating that the hopping of electrons was the possible mechanism responsible for conduction in the ferrites. Clearly, the values decreased as the Zn-Zr contents (x) increased from 0.128 eV with x = 0 to 0.086 eV with x = 0.4. This was due to the more stable bonding between the $Fe^{3+}$ and $Fe^{2+}$ ions compared with that between the $Fe^{3+}$ and $Zr^{4+}$ ions [53]. Thus, the changes in the activation energy and Curie temperature may have been due to electron hopping and the occupancy of cations at tetrahedral and octahedral sites. The $Zn^{2+}$ ions occupied the tetrahedral site and the $Zr^{4+}$ ions occupied the octahedral sites. Similar results were obtained in previous studies [54, 55].

**Table 4**. Activation energies ($E_P$, $E_f$, and $\Delta E$) and Curie temperature ($T_c$) for $CZ^2FO$ samples with different Zn-Zr contents.

| Zn-Zr Content | Activation Energy (eV) (± 0.001) | | | ($T_c$) (K) |
|---|---|---|---|---|
| | $E_P$ | $E_f$ | $\Delta E$ | |
| 0.0 | 0.238 | 0.110 | 0.128 | 600 |
| 0.1 | 0.217 | 0.102 | 0.115 | 585 |
| 0.2 | 0.203 | 0.098 | 0.105 | 570 |
| 0.3 | 0.187 | 0.092 | 0.095 | 553 |
| 0.4 | 0.176 | 0.090 | 0.086 | 543 |

## 4. Conclusions

In this study, cobalt ferrites doped with $Zn^{2+}$ and $Zr^{4+}$ were prepared successfully via the sol–gel route. XRD analysis confirmed the formation of spinel phases in the ferrite crystals. The variations in the lattice parameter according to the Zn-Zr contents conformed to Vegard's law. The FTIR spectra contained two main bands corresponding to the spinel structure of ferrite. The frequencies of both bands changed slightly as the Zn-Zr contents increased. The variations in the frequencies of the bands were due to the distributions of the $Co^{2+}$, $Zn^{2+}$, $Zr^{4+}$, and $Fe^{3+}$ ions over the tetrahedral (A) and octahedral (B) sites. The elastic constants decreased as the Zn-Zr contents (x) increased. The addition of Zn-Zr decreased the elastic moduli, which reflected the strengthening of

the inter-atomic bonding. The dielectric constant and dielectric loss tangent also decreased as the electric field frequency increased. The calculated activation energy values showed that the hopping of electrons could explain the conduction in the ferrites. The occupancy of the tetrahedral site by $Zn^{2+}$ and the octahedral site by $Zr^{4+}$ ions reduced the Curie temperatures of the ferrites as the Zn-Zr contents increased. The extra $ZrO_2$ phase (x = 0.3) had no effects on the properties of the ferrites.

ACCEPTED MANUSCRIPT

**References**


[1] A.G. Abraham, A. Manikandan, E. Manikandan, S.K. Jaganathan, A. Baykal, P.S. Renganathan, J. Nanoelectron. Optoelectron. 12 (2017) 1326.

[2] E. Hema, A. Manikandan, P. Karthika, M. Durka, S.A. Antony, B.R. Venkatraman, J. Nanosci. Nanotech. 16 (2016) 7325.

[3] S. Asiri, M. Sertkol, S. Guner, H. Gungunes, K.M. Batoo, T.A. Saleh, H. Sozeri, M.A. Almessiere, A. Manikandan, A. Baykal, Ceram. Int. 44 (2018) 5751.

[4] E. Hema, A. Manikandan, M. Gayathri, M. Durka, S.A. Antony, B.R. Venkatraman, J. Nanosci. Nanotechnol. 16 (2016) 5929.

[5] A.T. Ravichandran, J. Srinivas, R. Karthick, A. Manikandan, A. Baykal, Ceramics International 44 (2018) 13247.

[6] A. Silambarasu, A. Manikandan, K. Balakrishnan, J. Supercond. Novel Magn. 30 (2017) 2631.

[7] M. Maria Lumina Sonia, S. Anand, V. Maria Vinosel, M. Asisi Janifer, S. Pauline, A. Manikandan, Journal of Magnetism and Magnetic Materials 466 (2018) 238.

[8] S. Asiri, M. Sertkol, H. Güngüneş, Md. Amir, A. Manikandan, İ. Ercan, A. Baykal, Journal of Inorganic and Organometallic Polymers and Materials 28 (2018), 1587–1597.

[9] L. Lechevallier, J.M. Le Breton, J.F. Wang, I.R. Harris, J. Magn. Magn. Mater.269 (2004) 192.

[10] J. Sun, J. Li, G. Sun, J. Magn. Magn. Mater. 250 (2002) 20.

[11] M.A. Ahmed, E. Ateia, L.M. Salah, A.A. El-Gamal, Mater. Chem. Phys. 92 (2005) 310.

[12] D. Biswal, B.N. Peeples, C. Peeples, A.K. Pradhan, J. Magn. Magn. Mater. 345 (2013) 1–6.

[13] S.S. Jadhav, S.E. Shirsath, S.M. Patange, K.M. Jadhav, J. Appl. Phys. 108 (2010) 093920.

[14] M.A. Ahmed, N. Okasha, M. Gabal, Mater. Chem. Phys. 83 (2004) 107–113.

[15] A.K. Nikumbh, R.A. Pawar, D.V. Nighot, G.S. Gugale, M.D. Sangale, M.B. Khanvilkar, A.V. Nagawade, J. Magn. Magn. Mater. 355 (2014) 201.

[16] M.V. Reddy, D. Das, J. Alloys Compd. 634 (2015) 99.

[17] M.V. Reddy, A. Lisfi, S. Pokharel, D. Das, Sci. Rep.7 (2017) 7935.

[18] S.F. Rus, P. Vlazan, A. Herklotz, J. Nanosci. Nanotech., 16 (2016) 851.

[19] M. Popovici, C. Savii, D. Niznansky, J. Subrt, J. Bohacek, D. Becherescu, C. Caizer, C. Enache, C. Ionescu, J.Optoelectron.Adv.Mater.5 (2003) 251.

[20] I.H. Gul, A. Maqsood, J. Magn, Magn, Mater. 316 (2007) 13–18.

[21] Y.Y. Meng, Z.W. Liu, H.C. Dai, H.Y. Yu, D.C. Zheng, Powder Technol. 229 (2012) 270.

[22] A. Sutka, A. Borisova, J. Kleperis, G. Mezinskis, D. Jakovlevs, J. Aus. Ceram. Soc. 48 (2012) 150.

[23] S.M. Patange, S.S. Desai, S.S. Meena, S.M. Yusuf, S.E. Shirsath, RSC Adv. 5 (2015) 91482.

[24] R.K. Puri, U. Varshney, J. Phys. Chem. Solid.44 (1983) 655.

[25] D.G. Agresti, T.D. Shelfer, Y.K. Hong, Y.J. Paig, IEEE Trans. Magn.25 (1989) 4069.

[26] M.J. Iqbal, M.R. Siddiquah, J. Magn. Magn. Mater. 320 (2008) 845.

[27] S.M. Patange, S.E. Shirsath, B.G. Toksha, S.S. Jadhav, S.J. Shukla, K.M. Jadhav, Appl Phys A95 (2009) 429.

[28] V. Syepelak, I. Bergmann, A. Feldhoff, P. Heitjans, F. Krumeich, D. Menzel, F.J. Litterst, S.J. Campbell, K.D. Becker, J. Phys. Chem. C11 (2007) 50261.

[29] R.S. Shinde, P. Pareek, R. Yadav Proc. APAC, Gyeongju, Korea 2004702.

[30] M.S. Jebeli, N.M.B. Mohamed, Int. J. Mater. Sci. Innov.1 (2013) 45.

[31] M. Kumar, V.R. Gupta, S.K. Rout, Prog. Electromagn. Res. B 57 (2014) 157.

[32] V.L.O. Brito, A.C.C. Migliano, L.V. Lemos, F.C.L. Melo, Prog. Electromagn. Res. 91 (2009) 303.

[33] M.K. Zate, V.V. Jadhav, S.K. Gore, J.H. Shendkar, S.U. Ekar, A. Al-Osta, M. Naushad, R.S. Mane, J. Anal. Appl. Pyro.122 (2016) 224.

[34] A. Silambarasu, A. Manikandan, K. Balakrishnan, S.K. Jaganathan, E. Manikandan, J.S. Aanand, J. Nanosci. Nanotechnol. 18 (2018) 3523.

[35] M.M.L. Sonia, S. Anand, S. Blessi, S. Pauline, A. Manikandan, Ceramics International 44 (2018) 22068–22079.

[36] S.K. Gore, S.S. Jadhav, U.B. Tumberphale, S.M. Shaikh, M. Naushad, R.S. Mane, Solid Stat. Sci.74 (2017) 88.

[37] S.E. Shirsath, D. Wang, S.S. Jadhav, M.L. Mane, S. Li, Ferrites obtained by sol-gel method, Handbook of Sol-gel Science and Technology, Springer International Publishing AG, 2018, pp. 1–41.

[38] A.B. Mugutkar, S.K. Gore, R.S. Mane, K.M. Batoo, S.F. Adil, S.S. Jadhav, Ceram. Int. 44 (2018) 21675–21683.

[39] A. Dias, R.L. Moreira, Mater. Lett. 39 (1999) 69.

[40] S.T. Bishay, J. Magn. Magn. Mater. 301 (2006) 231.

[41] S.K. Gore, S.S. Jadhav, V.V. Jadahv, S.M. Patange, M. Naushad, R.S. Mane, K.H. Kim, Sci. Rep.7 (2017) 1524.

[42] N.C.S. Selvam, A. Manikandan, L.J. Kennedy, J.J. Vijaya, Journal of Colloid and Interface Science 389 (2013) 91–98.

[43] A. Manikandan, N.C.S. Selvam, L.J. Kennedy, R.T. Kumar, J.J. Vijaya, J. Nanosci. Nanotechnol. 13 (2013) 2595.

[44] A. Manikandan, J.J. Vijaya, L.J. Kennedy, Advanced Materials Research 699 (2013) 524.

[45] A. Manikandan, S.A. Antony, Synthesis and Reactivity in Inorganic, Metal-Organic, and Nano-Metal Chemistry, 46 (2016) 1277.

[46] S. Suguna, S. Shankar, S.K. Jaganathan, A. Manikandan, J. Nanosci. Nanotechnol. 18 (2018) 1019.

[47] S.S. Jadhav, S.E. Shirsath, B.G. Toksha, S.M. Patange, S.J. Shukla, K.M. Jadhav, Int. J. Mod. Phys. B 23 (2009) 5629.

[48] S. Singhal, J. Kaur, T. Namgyal, R. Sharma, Phys. B 407 (2012) 1223.

[49] S.G. Algude, S.M. Patange, S.E. Shirsath, D.R. Mane, K.M. Jadhav, J. Magn. Magn. Mater. 350 (2014) 39.

[50] Y.C. Venudhar, K.S. Mohan, Mater. Lett.55 (2002) 196.

[51] S.S. Jadhav, S.E. Shirsath, B.G. Toksha, D.R. Shengule, K.M. Jadhav, J. Opt. Elect. Adv. Mater.10 (2008) 2644.

[52] S. Kumar, G. Kumar, R.K. Kotnala, A. Kumar, P. Dhiman, M. Singh, Appld. Sci. Lett. 3 (2017) 20.

[53] L.Z. Li, X.X. Zhong, R. Wang, X.Q. Tu, J. Magn. Magn. Mater. 435 (2017) 58–63.

[54] A. Rasheed, M. Mahmood, U. Ali, M. Shahid, I. Shakir, S. Haider, M.A. Khan, M.F. Warsi, Ceram. Int. 42 (2016) 15747.

[55] S.K. Gurav, S.E. Shirsath, R.H. Kadam, S.M. Patange, K.S. Lohar, D.R. Mane, Mater. Res. Bull. 48 (2013) 3530.

ACCEPTED MANUSCRIPT

ACCEPTED MANUSCRIPT

**Highlights**

- Zn-Zr doped Co-ferrites.
- Conduction by electron hopping.
- Properties modified by doping.

ACCEPTED MANUSCRIPT